Atom-Scale Reaction Pathways and Free-Energy Landscapes in Oxygen Plasma Etching of Graphene

ARTICLE *in* JOURNAL OF PHYSICAL CHEMISTRY LETTERS · APRIL 2013

Impact Factor: 7.46 · DOI: 10.1021/jz400666h

4 AUTHORS:

Kenichi Koizumi
Institute for Molecular Science
45 PUBLICATIONS **533** CITATIONS
SEE PROFILE

Mauro Boero
Institut de Physique et Chimie des Matériaux d…
187 PUBLICATIONS **3,480** CITATIONS
SEE PROFILE

Yasuteru Shigeta
University of Tsukuba
174 PUBLICATIONS **1,837** CITATIONS
SEE PROFILE

Atsushi Oshiyama
The University of Tokyo
266 PUBLICATIONS **8,761** CITATIONS
SEE PROFILE

THE JOURNAL OF PHYSICAL CHEMISTRY Letters

Letter

pubs.acs.org/JPCL

Atom-Scale Reaction Pathways and Free-Energy Landscapes in Oxygen Plasma Etching of Graphene

Kenichi Koizumi,*[,†] Mauro Boero,[‡] Yasuteru Shigeta,[¶] and Atsushi Oshiyama[†]

[†]Department of Applied Physics, The University of Tokyo, Hongo, Tokyo 113-8656, Japan

[‡]IPCMS, CNRS, and University of Strasbourg, UMR 7504, F-67034 Strasbourg cedex 2, France

[¶]Department of Materials Engineering Science, Osaka University, Toyonaka, Osaka 560-8531, Japan

ABSTRACT: We report first-principles molecular dynamics calculations combined with rare events sampling techniques that clarify atom-scale mechanisms of oxygen plasma etching of graphene. The obtained reaction pathways and associated free-energy landscapes show that the etching proceeds near vacancies via a two-step mechanism, formation of precursor lactone structures and the subsequent exclusive CO_2 desorption. We find that atomic oxygen among the plasma components is most efficient for etching, providing a guidline in tuning the plasma conditions.

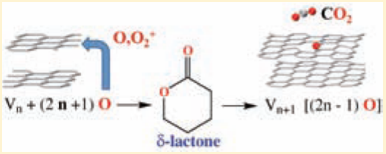

SECTION: Kinetics and Dynamics

Etching is a process to cut solid surfaces to make desired shapes. It has been utilized to create artistic design for many centuries. Combined with other techniques in current technology, it is now a powerful tool to fabricate submicrometer-scale devices.[1] To advance the etching technique satisfying requirements in nanoelectronics, however, the atom-scale control endorsed by quantum theory is imperative. Clarification of etching processes by first-principles calculations is thus highly demanded. We here report Car–Parrinello molecular dynamics (CPMD)[2] calculations that clarify mechanisms of the etching processes and provide the free-energy landscapes, taking graphene as an important example.

Fascinating properties of graphene such as an anomalous quantum Hall effect[3,4] and the unexpected magnetic ordering near edges[5−7] as well as the in-plane high mobility intrinsic to graphite place graphene as an emerging material to develop post-scaling technology challenged by the cutting-edge miniaturization.[1,3,8,9] To exploit the fascination that is essentially related to nanoscale shapes[10] of graphene, several experimental efforts have been done to produce desired geometries,[11−13] in which oxygen plasma etching (OPE) is one of the central fabrication techniques. Important issues to be clarified in OPE are reaction pathways in which C atoms are removed by attacking oxygen, resultant nanoshapes of graphene, and controllability of nanoscale etching. Such knowledge about OPE is totally lacking, however.

At the atomic scale, OPE of graphene is a reaction involving breaking and forming of chemical bonds among C atoms and oxygen plasma components. Therefore, to reveal its mechanism, dynamical approaches based on quantum theory, which is capable of accounting for changes in electronic structures during the reaction, are imperative. Yet standard first-principle dynamical simulations are incapable of tracing the bond reformation processes within the reachable time scale due to relatively high free-energy barriers. In this work, to overcome the difficulty, we resort to CPMD[2,14] combined with phase-space sampling techniques, named blue moon constrained dynamics[15] and metadynamics.[16−18] We then reveal for the first time the atom-scale processes of OPE of graphene and corresponding free-energy landscapes. We find that a two-step mechanism in which intrinsic vacancies in graphene and particular oxygen plasma components form lactone functional groups followed by irreversible CO_2 release is dominant in OPE.

In our calculations, electron interactions are treated by the generalized gradient approximation[19] in density functional theory,[20,21] complemented by Grimme's van der Waals corrections.[22] These, although not relevant for chemical reactions involving C and O, are essential for the interaction between graphene sheets.[24] In our simulated system, an A–B stacking graphene bilayer of 12.25 × 12.74 Å^2 lateral area is adopted, amounting to 120 C atoms. A vacuum layer of 11.0 Å is introduced along the third direction to allow for a good separation of repeated images and provides the space necessary for the insertion of the approaching plasma components.

Nuclei and core electrons are simulated by norm-conserving pseudopotentials.[23] Valence electron charge density is expanded in a plane wave basis set with a cutoff energy of 70 Ry and limited to the Γ point only because the lateral area is wide enough to ensure a good sampling of the Brillouin zone.[24] The ionic temperature (300 K) is controlled by a Nosé–Hoover thermostat[25−27] in all of our (*NVT*) simulations. The components of an oxygen plasma are an important issue and have been identified experimentally in a pressure range from 3 to 100 GPa as atomic oxygen (O) and charged molecular oxygen (O_2^+),[28] on which we focus here.

Received: March 26, 2013
Accepted: April 24, 2013
Published: April 24, 2013

dx.doi.org/10.1021/jz400666h | *J. Phys. Chem. Lett.* 2013, 4, 1592–1596

A first set of simulations targeting the approach of O to a perfect graphene surface has shown that O can stick on the surface, forming a stable epoxy form, which is consistent with previous static calculations.[29−31] Our constrained dynamical calculations then show that the free-energy profiles in the subsequent CO desorption monotonically increase with a barrier of 4.8 eV. Clarifying the robustness of the perfect graphene, we then focus on vacancies. Atomic vacancies in hexagonally bonded carbon sheets show peculiar characteristics,[32] that is, in the odd-number vacancy V_{2n+1}, there remains a dangling bond (DB) after rebonding of surrounding even-number atoms, whereas the even-number vacancy V_{2n} exhibits complete rebonding with annihilation of DBs. Therefore, the examination of the monovacancy V_1 and the divacancy V_2 covers the whole scenario in OPE of graphene.

O-Atom Reaction With V_1. Our unconstrained dynamics shows that one O atom added at 3.0 Å above the V_1 binds in a barrierless way to the C site carrying the DB. This gives rise to a C−O adduct protruding above the surface in a structure, shown in Figure 1a. We then explore a possibility that this CO moiety

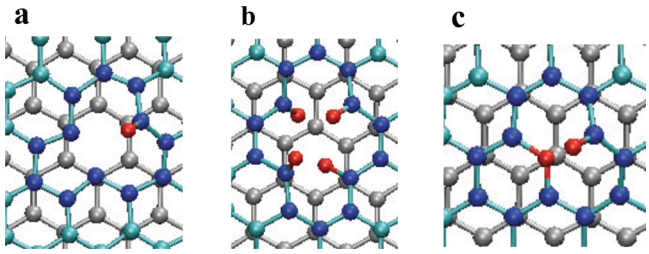

Figure 1. Atomic structures of oxygen-attacked vacancies in graphene. (a) The O-attacked V_1. (b) The O-attacked and then oxidized V_2. (c) The O_2^+-attacked V_1. The red, blue, and gray balls depict O and the first-layer and the second-layer C atoms, respectively.

desorbs as carbon monoxide by using the blue moon approach. In the simulation, we use as a reaction coordinate the coordination number[33] of the C atom of the C−O adduct with its two bonded C atoms belonging to the graphene sheet. This constrained dynamics has shown that the free-energy barrier for CO to desorb is larger than 4.5 eV, thus ruling out this pathway. This indicates that desorption of CO is unlikely to occur and that the OPE process must be realized by alternative pathways.

O-Atom Reaction with V_2. We have also performed unconstrained dynamics, adding an atomic O at 3.0 Å above the V_2 in which DBs are absent with the formation of two pentagons and a single octagon.[34] In this case, we find that the O atom attacks spontaneously one of the two rebonds in ∼2 ps, basically substituting for one of the two missing C atoms. This restores the hexagon and generates an ether-like functional group. Having already ruled out CO desorption, we do not attempt any extraction of CO. Instead, we have added another atomic O, within the same unconstrained dynamics approach, to explore reaction pathways. This second O atom goes spontaneously close to the remaining rebonded C−C atoms of the V_2. We are then left with two C−O−C ether adducts. Then, upon addition of two atomic oxygen, a subsequent reaction occurs. For the charged O_2^+ species, any attempt at observing a reaction with unconstrained dynamics has not succeeded within 3.0 ps at 300 K for both the V_1 and V_2. By examining the electronic structure, we notice that the doublet state of O_2^+ (as opposed to the triplet ground state of O_2) is carrying a hole h^+ in the spin density, and this is not keen on interacting with the DB of the V_1 or with the rebonds of the V_2. Both vacancies indeed are electron acceptors, and they spontaneously react with electron-rich reactants, such as O, but not with the h^+-rich O_2^+. As a result, O_2^+ fluctuates at around 5.0 Å above the vacancy but is inert during the whole simulation. To inspect the reaction barrier, we have then imposed as a reaction coordinate the distance between the centers of mass of the O_2^+ and the vacancy. By gradually shortening the distance, the free-energy barriers ΔF for O_2^+ adsorption are found to be ∼1.0 eV for the V_2 and 0.07 eV for the V_1.

V_1 versus V_2. The free-energy barriers obtained above show that the V_1 is much more reactive to the O_2^+ component than the V_2. The origin of this tendency is in the up and down spin states of the O_2^+ and of the DB of the V_1. These spin states tend to combine in a closed shell and make a stable C−O chemical bond. Interestingly, this occurs at the expenses of the already

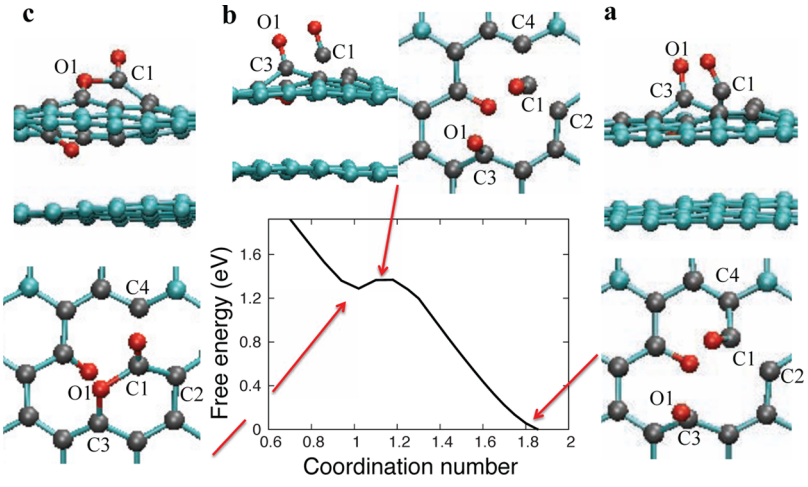

Figure 2. Free-energy profile of the lactone formation from an oxidized V_1. The abscissa is the coordination number of C1 with C2 and C4. Atomic structures of (a) the initial V_1 with an O and an O_2^+, (b) the transition state with a broken C1−C4 bond, and (c) the metastable state with the lactone form, that is, the C3−O1 group binds to the C1 carbon with another O, are shown. Gray balls indicate C atoms around the monovacancy, while other C sites are in cyan and O atoms in red. The second layer of graphene is not shown for clarity in the top views.

dx.doi.org/10.1021/jz400666h | J. Phys. Chem. Lett. 2013, 4, 1592−1596

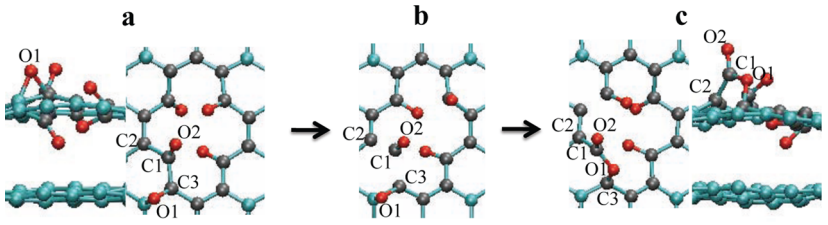

Figure 3. Reaction pathway for the formation of a lactone group in the V_2. The color code is identical to that in Figure 2. Atoms in the second layer are not shown for clarity in the top views. (a) Initial state with five O atoms bonded to C sites around the vacancy. (b) Transition state located at ΔF = 1.7 eV above (a). (c) Metastable final lactone-like structure at ΔF = 1.6 eV.

weakened O−O bond of O_2^+. We have indeed observed the cleavage of the O−O bond during the simulation followed by transfer of the edge O in the C−O−O group to one of the two remaining C atoms near the vacant site. The reached geometry shown in Figure 1c presents a C−O−C ether group and a nearby C−O. For the V_2, O_2^+ attacks, one of the four rebonded C atoms and then the O−O bond of the C−O−O adduct break for the reasons mentioned above. Eventually, one O atom is trapped in a C−O−C ether form, and the other O atom is absorbed on the graphene surface with the epoxy form. The reaction patterns obtained here for the V_1 and the V_2 are valid for the odd-number and the even-number vacancies, respectively, considering the local structural characteristics common to the vacancies.

Precursor for the Etching near V_1. Considering high reactivity of the O atom, we further explore the reaction when additional atomic O is added to the V_1 already adsorbed with the O_2^+ (Figure 1c). Starting with an O atom at 3.0 Å above the V_1, our unconstrained dynamics has shown that the O spontaneously attacks the O atom bridging two C sites (C−O−C) in a few picoseconds. Very rapidly, one of the two C−O bonds breaks with a temporary formation of a COO group, and then, the O−O bond is cleaved. A snapshot of the final structures is shown in Figure 2a, where all three C atoms around the V_1 hold one O atom with two CO groups pointing above the graphene surface and one on the sheet plane. To inspect a possibility of CO desorption from this oxidized V_1, we have performed the blue moon dynamics in which the coordination number of the C1 atom with C2 and C4 (Figure 2a) is gradually decreased. The obtained free-energy profile is shown in Figure 2. Namely, a transition state (Figure 2b) is formed upon breaking the C1−C4 bond, and then a metastable structure (Figure 2c) in which C1 binds to O1 appears. The associated free-energy barrier is 1.4 eV. Instead of the CO desorption, we have reached the metastable structure characterized as the lactone unit,which is a precursor structure for the CO_2 desorption.

Precursor for the Etching near V_2. After oxidation of V_2 with four O atoms (Figure 1b), none of the four C−O adducts is in a lactone form, implying that the subsequent CO desorption costs 4−5 eV. We then add another O to the structure and search for a stable geometry. The structure that we obtained is shown in Figure 3a, again lacking the CO_2 precursor. We then tried to release the CO unit next to the epoxy part, that is, C1−O2 in Figure 3a, via blue moon simulations by using a coordination number constraint on C1 with respect to the bonded C2 and C3. During the release process, as in the V_1 case, the nearby O1 oxygen approaches C1, and upon crossing a barrier ΔF = 1.7 eV (Figure 3b), a metastable minimum located at 1.6 eV above the initial structure is realized (Figure 3c). In this geometry, one CO_2 adduct is formed and kept bound to the sheet by the C1−C2 and O1−C3 bonds, similar to the V_1 case (Figure 2c).

The above two blue moon simulations are indicative that the CO desorption is hindered and instead the precursor lactone structure is formed with the free-energy barrier of about 1.5 eV.

Etching with CO_2 Desorption. We then focus on how graphene is etched from the precursor structures obtained above. Metadynamics is used to describe the processes involving multiple reaction coordinates. In the precursor lactone-like structure of V_1 (Figure 2c), a CO_2 adduct is bound to graphene by two chemical bonds, O1−C3 and C1−C2. Hence, we use the coordination numbers of O1 with C3 and of C1 with C2 as collective variables (CVs). The free-energy surface (FES) (Figure 4a) shows that the CO_2 adduct desorbs from graphene

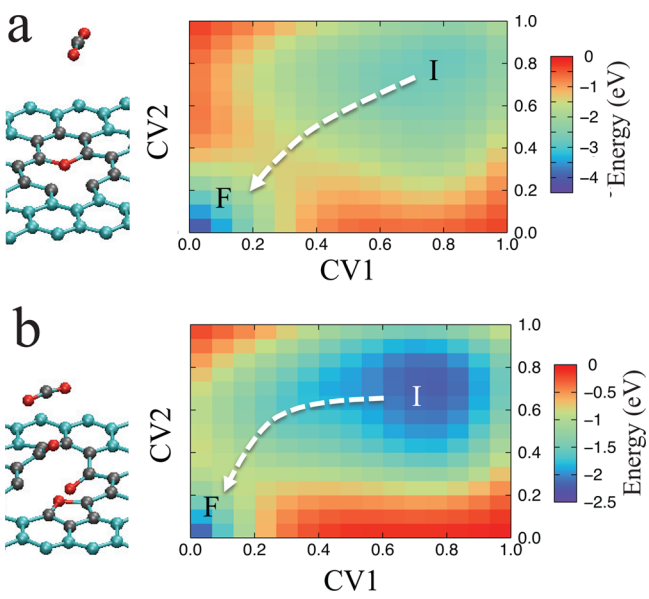

Figure 4. Free-energy landscape in the plane of the collective variables, CV1 and CV2 (see text), for the CO_2 desorption from graphene near (a) V_1 and (b) V_2. The initial precursor states, which are shown in Figure 2c and Figure 3c for the cases of the V_1 and V_2, respectively, are marked as I in the CV space, whereas the final desorbed state is marked as F. The atomic structures of the final states are shown in the left parts.

by overcoming a free-energy barrier of 1.3 eV. The two chemical bonds break in a concerted way, and there are two minima on the FES. The final desorbed state shown in the left of Figure 4a is characterized by a free energy lower than that of the initial precursor state by 1.6 eV. This ensures the irreversible release of CO_2 upon OPE. We have found that V_1 transforms into V_2 after the CO_2 desorption, showing an ether C−O−C geometry and a rebonded C−C. This resultant

dx.doi.org/10.1021/jz400666h | J. Phys. Chem. Lett. 2013, 4, 1592−1596

structure is essentially identical to the initial structure of V_2 attacked by an O atom, as shown at the beginning, indicative that subsequent etching processes proceed. We have also performed a second metadynamics simulation using as CVs the distances O1−C3 and C1−C2. This metadynamics also leads to the CO_2 desorption in an essentially identical way with the free-energy barrier of 1.3 eV.

In the precursor state for the V_2, the CO_2 adduct is trapped also in a lactone-like geometry (Figure 3c). We start metadynamics simulations from this precursor state using as CVs either the coordination numbers of C1 with C2 and of O1 with C3 or, alternatively, the distances C1−C2 and O1−C3. The FES obtained by using the coordination numbers as CVs is shown in Figure 4b. Both metadynamics simulations result in almost similar pathways with an activation barriers of about 1.4 eV, and the desorbed CO_2 state, shown on the left in Figure 4b, is more stable than the precursor state by about 0.3 eV. After the CO_2 desorption, the remaining trivacancy structure (the left in Figure 4b) exhibits a characteristic feature (i.e., an ether group and a C−O−C adduct) in V_1, or more generally in the odd-number vacancy, attacked by the initial oxygen, ensuring the subsequent etching of graphene. The projected free-energy profiles (not shown), computed as

$$F(s_i) = -k_B T \ln\left[\frac{\int \exp(-F(s_i, s_j)/k_B T)\, ds_j}{\int ds_j}\right] \quad (1)$$

where T is the temperature, k_B is the Boltzmann constant, and i,j = 1,2 indicates each collective variable; the CVs contribute in equal amount to the FES, confirming that no one is the dominating rate-limiting step and that both play an equally important role.

These barriers for CO_2 desorption are drastically lower than the 4.5 eV barrier for CO desorption, indicating that CO_2 is the dominant desorbed species.[35] Thus, the present results allow one to infer the following general pathway

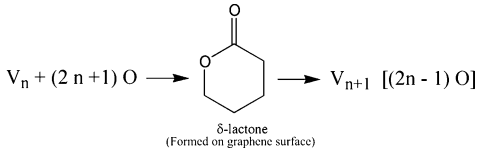

consisting first of the formation of a precursor lactone functional group and subsequently an irreveresible CO_2 with activation barriers of 1.3−1.4 eV. We remark also that the second perfect graphene layer is never attacked by oxygen at any stage of our simulations, thus supporting the notion of a layer-by-layer etching.[12]

In summary we have clarified the atom-scale mechanisms of the OPE of graphene by CPMD combined with the metadynamics and the blue moon approach. We show that perfect graphene is hard to etch,[36] whereas vacancies are easily attacked followed by the CO_2 desorption, hence answering the long-standing question about the desorbed species.[37] Atomic O in the plasma components etches graphene from vacant sites either with or without dangling bonds, while the O_2^+ component attacks vacant sites with dangling bonds. Because the even-number vacancies rebond perfectly, our study clearly indicates that an efficient plasma for OPE is the one in which atomic O is the major component, a major issue in designing plasma devices. Finally, a two-step mechanism has been evidenced and shown to hold for each kind of vacancy, thus offering a general scheme for graphene etching. Hence, it provids a useful guideline in designing and optimizing graphene etching processes.

AUTHOR INFORMATION

Corresponding Author

*E-mail: koizumi@comas.t.u-tokyo.ac.jp.

Notes

The authors declare no competing financial interest.

ACKNOWLEDGMENTS

This work is supported by a grant-in-aid project under Contact No. 22104005 and by CMSI, conducted by MEXT, Japan. Computations were done at ISSP, University of Tokyo, RCCS, National Institutes of Natural Sciences, and GENCI under Allocation x2012096092.

REFERENCES

(1) *International Technology Rodamap for Semiconductors*. http://www.itrs.net/ (2013).
(2) Car, R.; Parrinello, M. Unified Approach for Molecular Dynamics and Density-Functional Theory. *Phys. Rev. Lett.* **1985**, *55*, 2471−2474.
(3) Novoselov, K. S.; Geim, A. K.; Morozov, S. V.; Jiang, D.; Katsnelson, M. L.; Grigorieva, I. V.; Dubonos, S. V.; Firsov, A. A. Two-Dimensional Gas of Massless Dirac Fermions in Graphene. *Nature* **2005**, *438*, 197−200.
(4) Zhang, Y.; Tan, Y.-W.; Stormer, H. L.; Kim, P. Experimental Observation of the Quantum Hall Effect and Berry's Phase in Graphene. *Nature* **2005**, *438*, 201−204.
(5) Okada, S.; Oshiyama, A. Magnetic Ordering in Hexagonally Bonded Sheets with First-Row Elements. *Phys. Rev. Lett.* **2001**, *87*, 146803.
(6) Son, Y.-W.; Cohen, M. L.; Louie, S. G. Half-Metallic Graphene Nanoribbons. *Nature* **2007**, *444*, 347−349.
(7) Fernandez-Rossier, J.; Palacios, J. J. Magnetism in Graphene Nanoislands. *Phys. Rev. Lett.* **2007**, *99*, 177204.
(8) Novoselov, K. S.; Geim, A. K.; Morozov, S. V.; Jiang, D.; Zhang, Y.; Dubonos, S. V.; Grigorieva, I. V.; Frirsov, A. A. Electric Field Effect in Atomically Thin Carbon Films. *Science* **2004**, *306*, 666−669.
(9) Ozaki, J.; Kimura, N.; Anahara, T.; Oya, A. Preparation and Oxygen Reduction Activity of BN-Doped Carbons. *Carbon* **2007**, *45*, 1847−1853.
(10) Oshiyama, A.; Okada, S. *The Oxford Handbook of Nanoscience and Technology*; Oxford University Press: New York, 2010; Vol. 2, p 94.
(11) Ci, L.; Song, L.; Jariwala, D.; Elías, A. L.; Gao, W.; Terrones, M.; Ajayan, P. M. Graphene Shape Control by Multistage Cutting and Transfer. *Adv. Mater.* **2009**, *21*, 4487−4491.
(12) Rao, F.; Li, W.; Dong, L. *Nanotechnology (IEEE-NANO), 11th IEEE Conference*; The Institute of Electrical and Electronics Engineers, Inc. (IEEE): New York, 2011; p 1201.
(13) Bai, J.; Zhong, X.; Jiang, S.; Huang, Y.; Duan, X. Graphene Nanomesh. *Nat. Nanotechnol.* **2010**, *5*, 190−194.
(14) *CPMD*; Copyright IBM Corp., 1990−2013 and MPI für Festkörperforschung: Stuttgart, 1997−2001.
(15) Sprik, M.; Ciccotti, G. Free Energy from Constrained Molecular Dynamics. *J. Chem. Phys.* **1998**, *109*, 7737−7744.
(16) Laio, A.; Parrinello, M. Escaping Free-Energy Minima. *Proc. Natl. Acad. Sci. U.S.A.* **2002**, *99*, 12562−12566.
(17) Iannuzzi, M.; Laio, A.; Parrinello, M. Efficient Exploration of Reactive Potential Energy Surfaces Using Car−Parrinello Molecular Dynamics. *Phys. Rev. Lett.* **2003**, *90*, 238302.
(18) Kamiya, K.; Boero, M.; Tateno, M.; Shiraishi, K.; Oshiyama, A. Possible Mechanism of Proton Transfer through Peptide Groups in the H-Pathway of the Bovine Cytochrome *c* Oxidase. *J. Am. Chem. Soc.* **2007**, *129*, 9663−9673.
(19) Perdew, J. P.; Burke, K.; Ernzerhof, M. Generalized Gradient Approximation Made Simple. *Phys. Rev. Lett.* **1996**, *77*, 3865−3868.

(20) Hohenberg, P.; Kohn, W. Inhomogeneous Electron Gas. *Phys. Rev.* **1964**, *136*, B864−B871.
(21) Kohn, W.; Sham, L. J. Self-Consistent Equations Including Exchange and Correlation Effects. *Phys. Rev.* **1965**, *140*, A1133−A1138.
(22) Grimme, S. Accurate Description of van der Waals Complexes by Density Functional Theory Including Empirical Corrections. *J. Comput. Chem.* **2004**, *25*, 1463−1473.
(23) Troullier, N.; Martins, J. L. Efficient Pseudopotentials for Plane-Wave Calculations. *Phys. Rev. B* **1991**, *43*, 1993−2006.
(24) Ikeda, T.; Boero, M.; Huang, S. F.; Terakura, K.; Oshima, M.; Ozaki, J. Carbon Alloy Catalysts: Active Sites for Oxygen Reduction Reaction. *J. Phys. Chem. C* **2008**, *112*, 14706−14709.
(25) Nosé, S. A Molecular Dynamics Method for Simulations in the Canonical Ensemble. *Mol. Phys.* **1984**, *52*, 255−268.
(26) Nosé, S. A Unified Formulation of the Constant Temperature Molecular Dynamics Methods. *J. Chem. Phys.* **1984**, *81*, 511−519.
(27) Hoover, W. G. Canonical Dynamics: Equilibrium Phase-Space Distributions. *Phys. Rev. A* **1985**, *31*, 1695−1697.
(28) Musil, J.; Matouš, J.; Rajský, A. Optical Emission Spectra from Microwave Oxygen Plasma Produced by Surfatron Discharge. *Czech. J. Phys.* **1993**, *43*, 533−540.
(29) Nourbakhsh, A.; Cantoro, M.; Vosch, T.; Pourtois, G.; Clemente, F.; van der Veen, M. H.; Hofkens, J.; Heyns, M. M.; De Gendt, S.; Sels, B. F. Bandgap Opening in Oxygen Plasma-Treated Graphene. *Nanotechnology* **2010**, *21*, 435203.
(30) Sun, T.; Fabris, S.; Baroni, S. Surface Precursors and Reaction Mechanisms for the Thermal Reduction of Graphene Basal Surfaces Oxidized by Atomic Oxygen. *J. Phys. Chem. C* **2011**, *115*, 4730−4737.
(31) Larciprete, R.; Lacovig, P.; Gardonio, S.; Baraldi, A.; Lizzit, S. Atomic Oxygen on Graphite: Chemical Characterization and Thermal Reduction. *J. Phys. Chem. C* **2012**, *116*, 9900−9908.
(32) Nishikawa, M.; Iwata, J.-I.; Oshiyama, A. Morphology of Vacancy Aggregates in Carbon Nanotubes: Thinning Control Due to Interwall Interaction. *Phys. Rev. B* **2010**, *81*, 205442.
(33) Sprik, M. Coordination Numbers as Reaction Coordinates in Constrained Molecular Dynamics. *Faraday Discuss.* **1998**, *110*, 437−445.
(34) Berber, S.; Oshiyama, A. Atomic and Electronic Structure of Divacancies in Carbon Nanotubes. *Phys. Rev. B* **2008**, *77*, 165405.
(35) Carlsson, J. M.; Hanke, F.; Linic, S.; Scheffler, M. Two-Step Mechanism for Low-Temperature Oxidation of Vacancies in Graphene. *Phys. Rev. Lett.* **2009**, *102*, 166104.
(36) Ogino, T.; Tsukamoto, T. In *Graphene Etching on Well-Defined Solid Surfaces in Physics and Applications of Graphene — Experiments*; Mikhailov S., Ed.; InTech Pubs.: New York; 2011, pp 91−108.
(37) Holland, L.; Ojha, S. M. The Chemical Sputtering of Graphite in an Oxygen Plasma. *Vacuum* **1976**, *26*, 53−60.